DOI: 10.19884/j.1672-5220.202304003

Visible Light-Activated Phosphorescence Systems Co-Assembled by Phenanthroline-Based Molecules with Polyvinyl Alcohol

ZHANG Taiguang*, LIU Dongliang, WU Hongwei
College of Chemistry and Chemical Engineering, Donghua University, Shanghai 201620, China

Abstract: Developing pure organic room-temperature phosphorescence (RTP) materials with visible light activation has drawn widespread attention. In this work, a visible light-activated RTP design strategy was developed by incorporating the phenanthroline-based donor-acceptor (D-A) phosphor into a rigid polymer matrix polyvinyl alcohol (PVA). Phenanthroline with rich heteroatom N can promote the generation of triplet excitons and form abundant hydrogen bonds with PVA, inhibiting the non-radiative relaxation and thereby leading to phosphorescence. Upon irradiation with 420 nm visible light, the phosphorescence color of these doped PVA films can be shifted from green to yellow by regulating the molecular conjugated structure and D-A interaction. Based on the phosphorescence properties, these doped PVA films can be used for information encryption. This work offers a simple and feasible approach for constructing visible light-activated phosphorescence materials with excellent application prospects in information encryption, sensors and other fields.

Key words: phosphorescence; phenanthroline; visible light; polymer system
CLC number: O631 **Document code**: A
Article ID: 1672-5220(2024)02-0137-09

Open Science Identity (OSID)

0 Introduction

Room-temperature phosphorescence (RTP) materials with rich triplet activated-state properties have gained considerable attention because of their long-lived luminescence and significant Stokes shift, and can be widely applied in information encryption and storage[1-2], bioimaging[3-4] and sensors[5]. Generally, some heavy atoms or heteroatoms with lone pair electrons are introduced into phosphors to enhance the intersystem crossing (ISC) efficiency for promoting the triplet excitons generation[6-7]. Meanwhile, rational strategies are also employed to construct a rigid environment that can weaken the nonradiative energy dissipation of phosphors, such as crystal engineering[8-10], polymerization[11-12], host-guest doping[13-14] and supramolecular assembly[15], thus favoring efficient RTP emission. Among them, the simple and common host-guest doping strategy is used to uniformly disperse a small amount of phosphors into a mass of host materials. For example, Sun et al.[16] developed a purely organic fluid material with RTP characteristics through strong hydrogen-bonding interactions between fluid host and commercial fluorescent molecules. Xiao et al.[17]. reported a host-guest doped crystal with the capability of on-off RTP, which could respond to hydrochloric acid stimuli through the switching halogen bonding. Additionally, Kwon et al.[18] constructed an amorphous purely organic RTP system by doping phosphors with a bromoaldehyde core and carboxylic acid side chains into a polyvinyl alcohol (PVA) matrix, and then the system exhibited the transformation from strong green phosphorescence to blue fluorescence under humidity stimuli. As the humidity increased, the water molecule could disrupt the hydrogen bonding interaction between PVA and phosphors, resulting in significantly decreased phosphorescence[18]. Notably, the transparent and flexible polymer-based RTP materials by embedding phosphors into various polymer matrices are highly suitable for simple, large-scale and reproducible production. Because of these excellent properties, developing the polymer-based RTP materials is highly desirable.

Generally, most polymer-based RTP materials are activated by ultraviolet (UV) light with high toxicity and poor penetrating ability. However, a few reports about RTP systems with visible light-activated characteristics typically rely on intermolecular aggregation rather than a

Received date: 2023-04-04
Foundation items: Shanghai Pujiang Program of China (No. 20PJ1400500); International Cooperation Fund of Science and Technology Commission of Shanghai Municipality, China (No. 21130750100); Fundamental Research Funds for the Central Universities, China (No. 2232022A-03)
* Correspondence should be addressed to ZHANG Taiguang, email: 2200761@mail.dhu.edu.cn
Citation: ZHANG T G, LIU D L, WU H W. Visible light-activated phosphorescence systems co-assembled by phenanthroline-based molecules with polyvinyl alcohol [J]. *Journal of Donghua University (English Edition)*, 2024, 41(2): 137-145.

monomer state[19-20]. For example, Cai et al.[21] achieved ultralong RTP with visible light activated by regulating molecular interactions. Notably, visible light-activated RTP based on the single-molecule state in polymer systems is rarely reported. Herein, a visible light-activated RTP design strategy by incorporating the phenanthroline-based donor-acceptor (D-A) phosphor into a rigid PVA matrix is developed. The phenanthroline and its derivatives possess a large π conjugated planar structure, and its heteroatom N can enhance the spin-orbit coupling (SOC) and further increase the generation of triplet excitons, promoting phosphorescence. At the same time, these heteroatoms could establish hydrogen bonds with the PVA matrix, and create a rigid environment for the guest phosphors, which could inhibit the non-radiative relaxation process. Additionally, the collaborative molecular design strategy of expanding molecular conjugation and replacing substituent groups endows these D-A phosphors with visible light-activated RTP characteristics, and the RTP could even reach the yellow region.

1 Materials and Methods

1.1 Materials

2-Bromo-1, 10-phenanthroline, 2-hydroxyphenylboronic acid, 6-hydroxy-2-naphthaleneboronic acid and tetrakis(triphenylphosphine) palladium were purchased from Shanghai Bide Pharmaceutical Technology Co. (Shanghai, China). Anhydrous potassium carbonate, petroleum ether, ethyl acetate, 1,4-dioxane, anhydrous sodium sulfate, deuterated dimethyl sulfoxide, deuterated chloroform, dichloromethane and anhydrous sodium sulfate were purchased from Shanghai Titan Technology Co. (Shanghai, China). 6-Methoxy-2-naphthaleneboronic acid was purchased from Shanghai Haohong Biopharmaceutical Technology Co. (Shanghai, China). Column chromatography silica gel was purchased from Yantai Jiangyou Silicone Development Co. (Yantai, China). PVA (M_w: 146 000−186 000) was purchased from Sigma-Aldrich Shanghai Trading Co., Ltd (Shanghai, China).

1.2 Synthesis of molecules A−C

1.2.1 Synthesis of molecule A

2-Bromo-1,10-phenanthroline (2.0 mmol, 0.518 2 g), 2-hydroxyphenylboronic acid (2.4 mmol, 0.331 0 g), tetrakis(triphenylphosphine) palladium (0.1 mmol) in 1, 4-dioxane (30 mL) and potassium carbonate (6 mmol, 0.552 8 g) in water (5 mL) were mixed. Then, this mixture was added to the three-necked flask and heated to reflux at 80 ℃ for 12 h under N_2 protection. At the end of the reaction, water was added to quench the reaction. The organic phase was extracted with ethyl acetate, and the excess water in the organic phase was removed by adding anhydrous sodium sulfate. After adding silica gel, the organic solvent was removed by a rotary evaporator. The sample was separated and purified by column chromatography (the volume ratio of petroleum ether to ethyl acetate was 6∶1). It was dried to give a solid yellow powder, named molecule **A**. The yield was 40 %. ^{1}H nuclear magnetic resonance (NMR) (400 MHz, DMSO-d_6) δ: 16.02 (s, 1H), 9.19 (dd, J = 4.4, 1.6 Hz, 1H), 8.77−8.61 (m, 2H), 8.58 (dd, J = 8.0, 6.4 Hz, 1H), 8.30 (dd, J = 8.0, 6.6 Hz, 1H), 8.13−8.04 (m, 2H), 7.86 (dd, J = 8.0, 4.2 Hz, 1H), 7.46−7.38 (m, 1H), 7.08−6.96 (m, 2H). ^{13}C NMR (101 MHz, DMSO-d_6) δ: 161.18, 157.14, 151.01, 144.07, 142.18, 138.72, 136.87, 132.50, 129.23, 127.79, 127.10, 126.99, 126.36, 124.33, 119.50, 118.94, 118.91, 118.85, 40.59, 40.38, 40.17, 39.97, 39.76, 39.55, 39.34.

1.2.2 Synthesis of molecule B

The procedure is similar to that of molecule **A**, except that the benzene ring in the reactant is replaced with a naphthalene ring. ^{1}H NMR (400 MHz, DMSO-d_6) δ: 9.97 (s, 1H), 9.20 (dd, J = 4.2, 1.8 Hz, 1H), 8.82 (d, J = 1.6 Hz, 1H), 8.61−8.49 (m, 4H), 8.07−7.95 (m, 3H), 7.90 (d, J = 8.8 Hz, 1H), 7.81 (dd, J = 8.0, 4.2 Hz, 1H), 7.24−7.14 (m, 2H). ^{13}C NMR (101 MHz, DMSO-d_6) δ: 156.85, 156.30, 150.34, 146.05, 145.76, 137.65, 136.72, 135.76, 133.65, 130.94, 129.31, 128.14, 127.71, 127.19, 126.99, 126.89, 126.66, 125.68, 123.71, 120.44, 119.63, 109.13, 40.57, 40.36, 40.15, 39.95, 39.74, 39.53, 39.32.

1.2.3 Synthesis of molecule C

The procedure is similar to that of molecule **A**, except that the donor part is modified to methoxy. ^{1}H NMR (400 MHz, Chloroform-d) δ: 9.31 (dd, J = 4.4, 1.6 Hz, 1H), 8.82 (d, J = 1.8 Hz, 1H), 8.54 (dd, J = 8.6, 2.0 Hz, 1H), 8.37−8.28 (m, 2H), 8.26 (d, J = 8.4 Hz, 1H), 7.99−7.90 (m, 2H), 7.87−7.76 (m, 2H), 7.69 (dd, J = 8.0, 4.4 Hz, 1H), 7.20 (dd, J = 8.0, 2.4 Hz, 2H), 3.97 (s, 3H). ^{13}C NMR (101 MHz, DMSO-d_6) δ: 158.57, 156.15, 150.39, 146.07, 145.78, 137.73, 136.72, 135.46, 134.52, 130.78, 129.32, 128.93, 127.81, 127.68, 127.07, 126.89, 126.79, 125.95, 123.75, 120.54, 119.56, 106.40, 55.73, 40.57, 40.37, 40.16, 39.95, 39.74, 39.53, 39.32.

2 Results and Discussion

2.1 Schematic illustration of visible light-activated RTP system

A visible light-activated RTP system was obtained by incorporating the phenanthroline-based D-A phosphor

and molecule **A**, **B** or **C** into a rigid PVA matrix. The schematic illustration of hydrogen bond nets of molecule **A**, **B** or **C** with PVA is shown in Fig. 1.

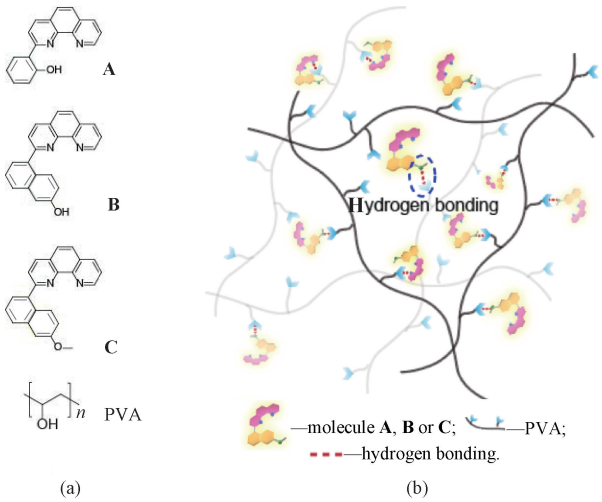

Fig. 1 Schematic illustration of hydrogen bond nets of phenanthroline-based D-A phosphor with PVA: (a) molecules **A**, **B**, **C** and PVA; (b) hydrogen bond nets

PVA films doped with molecule **A**, **B** or **C** were named as A-PVA, B-PVA or C-PVA, respectively. To be specific, 0.1 mg (1.0 mg, 3.0 mg and 6.0 mg) **A** mixed with 100 mg PVA was named as A-PVA-0.1 (A-PVA-1, A-PVA-3 and A-PVA-6); 0.1 mg (1.0 mg, 3.0 mg and 6.0 mg) **B** mixed with 100 mg PVA was named as B-PVA-0.1 (B-PVA-1, B-PVA-3 and B-PVA-6); 0.1 mg (1.0 mg, 3.0 mg and 6.0 mg) **C** mixed with 100 mg PVA was named as C-PVA-0.1 (C-PVA-1, C-PVA-3 and C-PVA-6).

2.2 Photophysical properties of A-PVA

According to Ref. [22], A-PVA with low-doped mass fraction, A-PVA-0.1, was selected to study the single-molecule state of phosphor in the film, and A-PVA with high-doped mass fraction, A-PVA-3, was selected to study the ultraviolet-visible (UV-vis) absorption properties. As shown in Fig. 2(a), the UV-vis absorption spectrum of A-PVA-0.1 indicates that the absorption peak is located at 290 nm. Its absorption band extends into the visible light region due to the D-A molecular structure, which facilitates the formation of the charge-transfer absorption band. A-PVA-3 also shows similar absorption characteristics but with a higher absorption intensity (Fig. 2(b)). The fluorescence characterization of A-PVA-0.1 is shown in Fig. 2(c). A-PVA-0.1 exhibits a green fluorescence emission peak at 490 nm, with a fluorescence lifetime τ of 4.7 ns. It is supposed that the green fluorescence stems from the single-molecule state of guest molecule **A** in keto form. However, A-PVA-3 displays a dual-fluorescence emission with prominent peaks at 500 and 615 nm (Fig. 2(d)). This phenomenon may be due to the formation of a molecular aggregation state at a high-doped mass fraction, resulting in prolonged wavelength emission with an emission peak at 615 nm. Due to the inhomogeneity of the high-doped mass fraction film, this film contains both single-molecule and aggregated state fluorescence. Furthermore, the different phosphorescence phenomena of A-PVA-0.1, A-PVA-1, A-PVA-3 and A-PVA-6 are compared. It is noted that the fluorescence intensity of A-PVA-1 achieves better results because of a lower doped mass fraction and stronger rigid environment (Fig. 2(e)). Simultaneously, along with the on or off of the 420 nm visible light, the film manifests decayed phosphorescence phenomena until the UV light is turned off for 1.0 s as shown in Fig. 2(g).

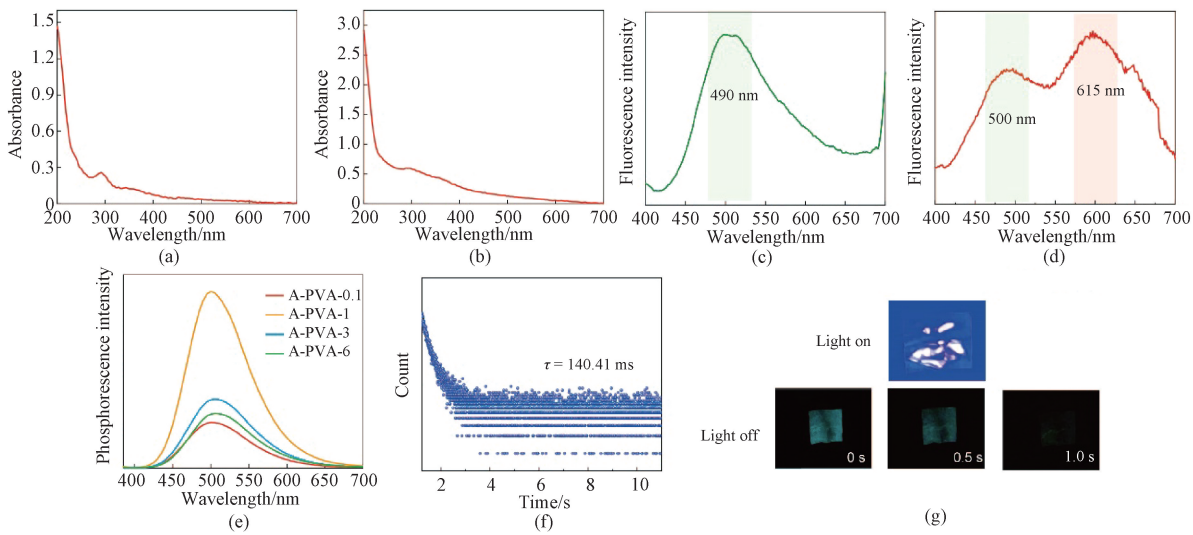

Fig. 2 Photophysical properties of A-PVA (λ = 420 nm): (a) UV-vis absorption spectrum of A-PVA-0.1; (b) UV-vis absorption spectrum of A-PVA-3; (c) fluorescence spectrum of A-PVA-0.1; (d) fluorescence spectrum of A-PVA-3; (e) phosphorescence spectra of A-PVA; (f) phosphorescence lifetime of A-PVA-1; (g) phosphorescence photographs of A-PVA-1

Then, the phosphorescence properties of A-PVA were investigated. A-PVA lead a green afterglow visible to the naked eye for 1.5 s after being activated by a 365 nm UV light. As shown in Fig. 2(e), A-PVA with low-doped and high-doped mass fractions all exhibit a single phosphorescence peak at about 500 nm, indicating that the phosphorescence emission of molecule **A** in these doped films is the single-molecule state. The CIE coordinate of A-PVA-1 is (0.23, 0.44), further indicating A-PVA have green phosphorescence. The phosphorescence intensity of A-PVA-1 is the strongest, however, its intensity subsequently decreases as the doped mass fraction increases. This phenomenon may be attributed to the molecular aggregation occurring at high-doped mass fractions, which leads to the quenching of some triplet excitons and facilitates energy transfer among these molecules. Additionally, the phosphorescence lifetime τ of A-PVA-1 at 500 nm is 140.41 ms, which proves its phosphorescence characteristic (Fig. 2(f)). Based on the UV-vis absorption spectra that are presented in Figs. 2(a) and 2(b), it is hypothesized that A-PVA may possess visible light-activated RTP characteristics. In order to verify this conjecture, a 420 nm visible light was adopted to activate A-PVA-1, as shown in Fig. 2(g). A green afterglow is observed by the naked eye after activation, which persists for about 1.0 s. Additionally, we attempted to activate this film by using a 455 nm visible light, but it was unsuccessful due to the low absorption of A-PVA at this wavelength. Furthermore, A-PVA-1 was analyzed by phosphorescence spectroscopy with visible light activation. The result presented in Fig. 2(e) demonstrates that A-PVA-1 displays green phosphorescence with a maximum wavelength of around 510 nm. It is worth noting that such visible light-activated RTP is rare in polymeric phosphorescence materials.

2.3 Photophysical properties of B-PVA

Due to the benzene ring with a small conjugation structure, the benzene ring was replaced with a naphthalene ring to expand the conjugated molecular structure, obtaining molecule **B**. It was anticipated that B-PVA exhibited a red-shift phosphorescence emission compared to A-PVA. The photophysical properties of B-PVA are shown in Fig. 3.

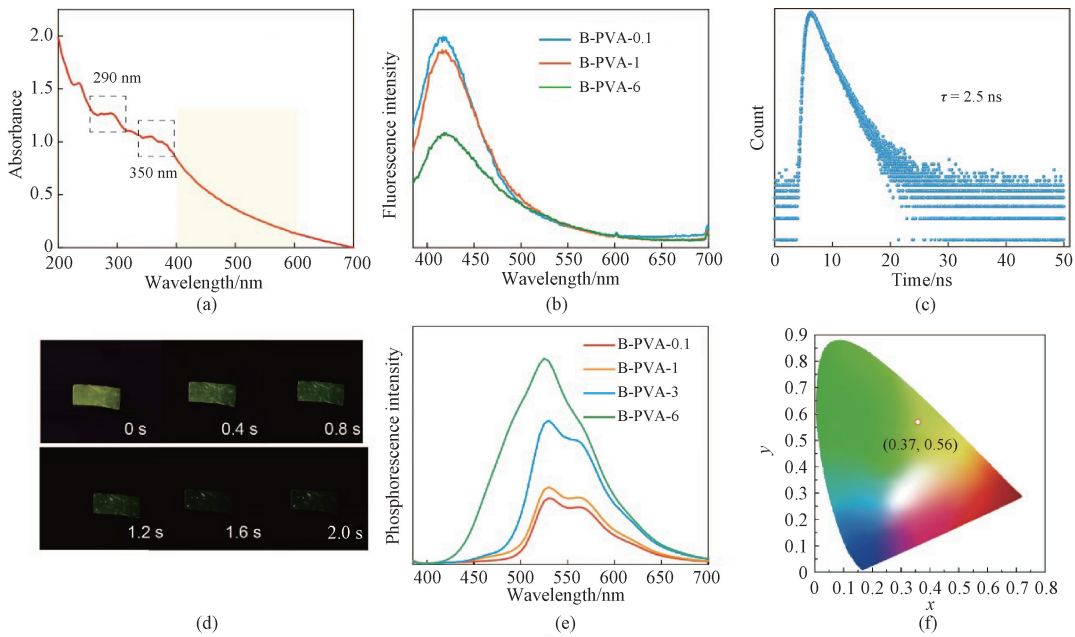

Fig. 3 Photophysical properties of B-PVA(λ = 365 nm): (a) UV-vis absorption spectrum of B-PVA-3; (b) fluorescence spectra of B-PVA; (c) fluorescence lifetime of B-PVA-0.1; (d) phosphorescence photographs of B-PVA-0.1(light off); (e) phosphorescence spectra of of B-PVA; (f) CIE coordinate diagram of B-PVA-0.1

As shown in Fig. 3(a), the characteristic absorption peaks are located at 290 and 350 nm, which extend the visible region, and indicate that B-PVA has the potential to activate RTP using visible light. B-PVA-0.1 possesses blue fluorescence around 418 nm with a lifetime τ of 2.5 ns (Figs. 3(b) and 3(c)). However, it should be noted that the fluorescence intensities decrease with an increase in the doped mass fraction because aggregation-induced fluorescence quenching occurs at molecule **B** with a high-doped mass fraction.

After irradiation with UV light at 365 nm, B-PVA-0.1 exhibites a yellow-green afterglow, and its dual-wavelength phosphorescence peaks center at 530 and 565 nm regardless of the molecular mass fraction, suggesting two vibrational peaks in the single-molecule state (Figs. 3(d) and 3(e)). The CIE coordinate of B-PVA-0.1 is (0.37, 0.56), further indicating its phosphorescence color is yellow-green (Fig. 3(f)). As expected, the phosphorescence of B-PVA indeed possesses a significant red shift compared with that of A-PVA.

Besides, its phosphorescence lifetime is also improved, lasting approximately about 2.0 s (Fig. 3(d)). The phosphorescence lifetime of B-PVA-0.1 at 530 nm (636.35 ms) is longer than that at 565 nm (137.72 ms). The differences in phosphorescence lifetime between different wavelengths can result in time-dependent changes in phosphorescence color. As shown in Fig. 3(d), the phosphorescence color of B-PVA-0.1 initially appeares close to yellow, and its phosphorescence color tends to become green over time.

Similar to molecule **A**, molecule **B** also retains the visible light-activated RTP properties. The phosphorescence properties and CIE coordinate diagram of B-PVA-3 are shown in Fig. 4.

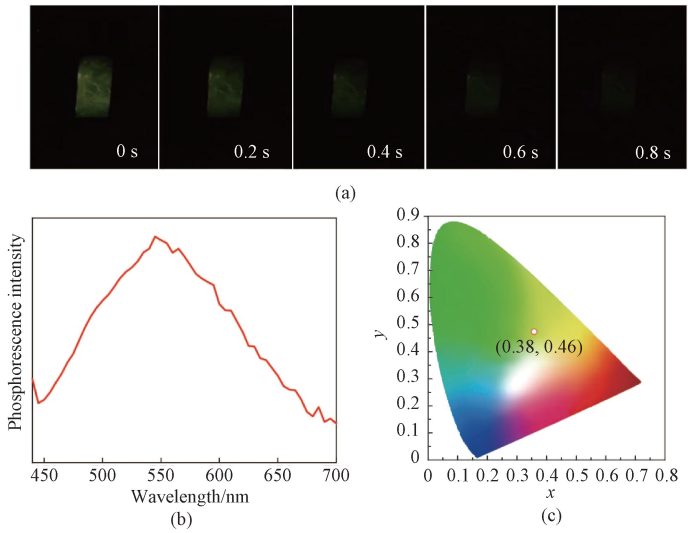

Fig. 4 Phosphorescence properties of B-PVA-3 (λ = 420 nm): (a) phosphorescence photographs (light off); (b) phosphorescence spectrum; (c) CIE coordinate diagram

After being activated by a 420 nm visible light, a yellow phosphorescence of B-PVA that lasts for approximately 0.8 s can be observed (Fig. 4(a)). At the same time, the 420 nm visible light-activated phosphorescence spectrum is characterized, and it displays a single phosphorescence peak located at 545 nm, which may be attributed to the longer-wavelength phosphorescence being more easily activated at this wavelength, thereby becoming the dominant emission (Fig. 4(b)). The CIE coordinate is (0.38, 0.46), further indicating that it is in the luminous yellow region, as depicted in Fig. 4(c).

2.4 Photophysical properties of C-PVA

While B-PVA are able to exhibit yellow RTP upon being activated by visible light, the phosphorescence emission intensity is relatively weak and the duration of phosphorescence is short. Therefore, the phenanthroline system based on molecule **B** is further improved by modifying the donor part to methoxy, resulting in molecule **C**. It is possible to modify the luminous performances by altering the electron-donating ability of substituent groups. In addition, the molecular solubility can be greatly improved when the hydroxyl group is substituted by the methoxyl group. The photophysical properties of C-PVA are shown in Fig. 5.

As shown in Fig. 5(a), both C-PVA-3 and C-PVA-0.1 exhibit similar absorption, and their absorption ranges extend to the visible region. The fluorescence spectra indicate that C-PVA with different doped mass fractions emit blue fluorescence under the activation by 365 nm UV light, and the fluorescence intensity increases gradually with the increase of the doped mass fractions (Fig. 5(b)). The maximum emission wavelength stays at 410 nm with a fluorescence lifetime τ of 2.5 ns. Interestingly, when the UV light is switched off, C-PVA-0.1 exhibits a yellow-green afterglow which can last for up to 6 s (Fig. 5(c)). C-PVA-0.1 exhibits dual-wavelength emission centered at 530 nm and 555 nm (Fig. 5(d)). This dual-wavelength emission phenomenon in a single-molecule state may also be caused by different vibrational states. With the increase of the doped mass fraction, the phosphorescence intensity continuously decreases due to the molecular aggregation which could quench triplet excitons. It is also observed that as the doped mass fraction increases, the emission peak at 555 nm is enhanced compared to that at 530 nm, and the phosphorescence of the high-doped mass fraction film is red-shifted (Fig. 5(d)). Compared with that of C-PVA-6, the phosphorescence of C-PVA-0.1 is more yellow, because the guest molecules at a higher-doped mass fraction may experience an environment that favors the low-energy vibrational dynamics emission. Based on its CIE coordinate of (0.37, 0.58), it can be inferred that the phosphorescence color is yellow-green (Fig. 5(e)). As for C-PVA-0.1, the fluorescence lifetimes τ at 530 and 555 nm are 692.91 and 703.25 ms, respectively (Fig. 5(f)). It can be observed that the phosphorescence lifetime of molecule **C** in the doped state is the longest among the three molecules. This is due to the stronger D-A interaction of molecule **C** which results in a longer-lived charge transfer state.

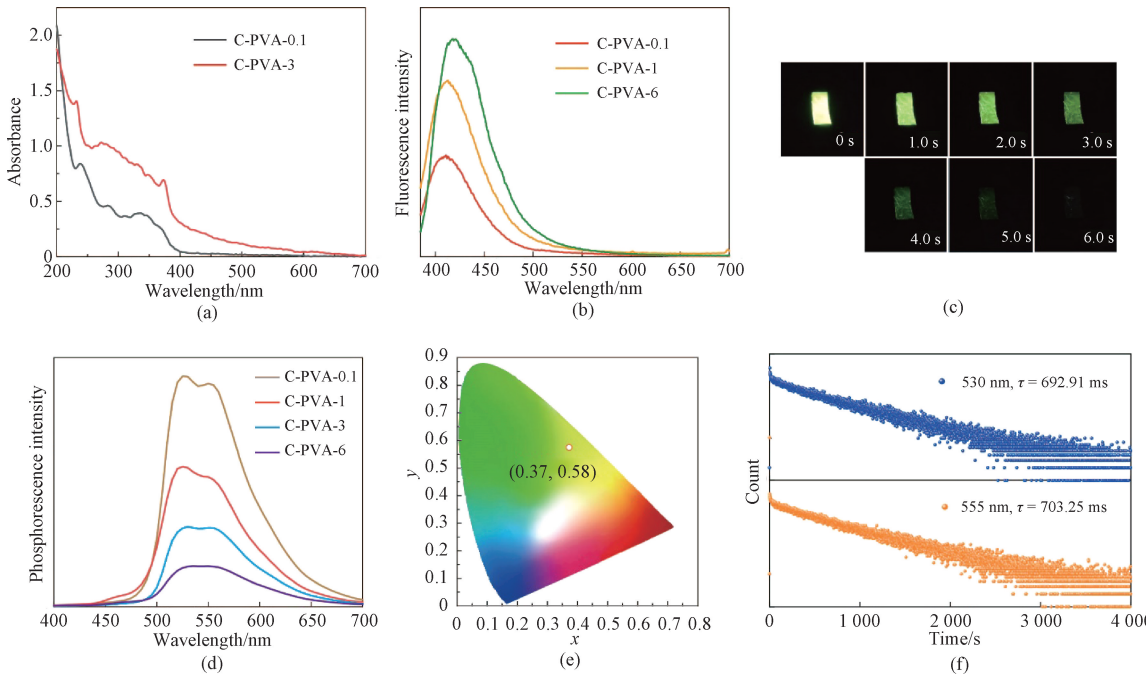

Fig. 5 Photophysical properties of C-PVA(λ = 365 nm): (a) UV-vis absorption spectra of C-PVA-0.1 and C-PVA-3; (b) fluorescence spectra of C-PVA; (c) phosphorescence photographs of C-PVA-0.1; (d) phosphorescence spectra of C-PVA; (e) CIE coordinate diagram of C-PVA-0.1; (f) phosphorescence lifetime of C-PVA-0.1

In addition, after turning off the visible light, C-PVA-0.1 exhibits a yellow-green afterglow which can last for up to 2 s (Fig. 6(a)). As can be seen from Fig. 6(a), C-PVA-0.1 also possesses the visible light-activated RTP characteristic. Compared with that of UV light activation, its phosphorescence spectrum activated by visible light shows a specific red shift, and the maximum emission peak is located at around 550 nm (Fig. 6(b)). The CIE coordinate diagram of C-PVA-0.1 shows that the color is closer to yellow, as evidenced by its CIE coordinate of (0.38, 0.48), consistent with the observed phenomena (Fig. 6(c)).

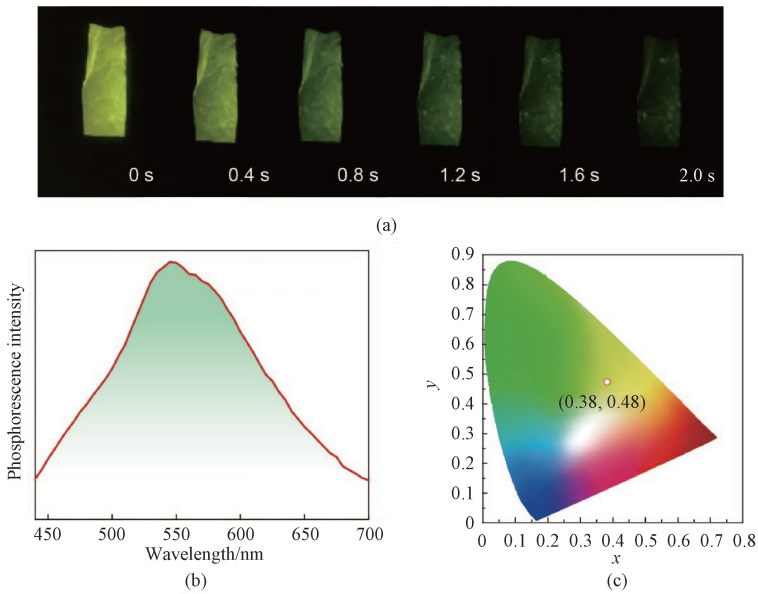

Fig. 6 Phosphorescence properties of C-PVA-0.1(λ = 420 nm): (a) phosphorescence photographs; (b) phosphorescence spectrum; (c) CIE coordinate diagram

2.5 Analysis of luminescence mechanism

After investigating the photophysical properties, we have gained an initial insights into the luminescence mechanism of these doped films. The luminescence mechanism of the phenanthroline-based doped film is shown in Fig. 7.

Along with energy absorption, the molecular energy level transitions from the grand state (S0) to the first singlet state (S1). The fluorescence luminous (FL) phenomena will be realized through energy level down (S1 to S0). Furthermore, the phosphorescence phenomena is achieved by two produces. One is the intersystem crossing (ISC). The energy level crosses from S1 to the first triplet state (T1). The other process involves the transition from T1 to S0, the energy level of which decreases along with the emission of phosphorescence. However, because of the nonradiation (NR), for example heat loss, part of the energy cannot be utilized for phosphorescence phenomena. It is well known that introducing appropriate heteroatoms into the molecule can promote the n-π transition, thereby enhancing the SOC, and is beneficial for the ISC process between singlet and triplet states, increasing the generation of triplet excitons and promoting the phosphorescence. Furthermore, doping these molecules into PVA matrix can create a hydrogen-bonding network, which establishes a rigid environment that can inhibit their NR relaxation process. By employing a rational molecular design strategy of expanding molecular conjugation and replacing substituent groups, these molecules can be endowed with different D-A structures, promoting charge transfer and obtaining visible light-activated RTP.

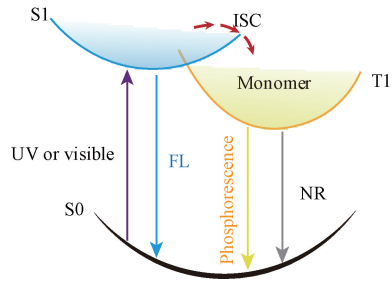

Fig. 7 Luminescence mechanism of phenanthroline-based doped film

2.6 Application potential

Currently, most yellow RTP materials are restricted to solid powders or crystallites, which limits their practical applications due to their lack of flexibility. Therefore, the yellow RTP material with excellent flexibility and transparency is developed as shown in Fig. 8. C-PVA is taken as an example to explore its application potential as shown in Fig. 9.

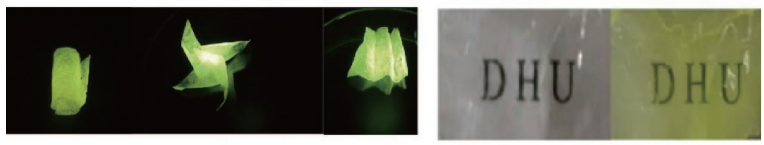

(a) (b)

Fig. 8 Various transparent objects based on phenanthroline-based doped films: (a) rolled, folded and bended films; (b) transparency of doped film

(a) (b) (c)

Fig. 9 Images of "DHU" on filter paper: (a) under 420 nm visible light; (b) 365 nm UV light irradiation on; (c) 360 nm UV light irradiation off

As shown in Fig. 8(a), C-PVA can be easily rolled, folded and bended, thus can be processed into various shapes. The films also exhibit bright yellow phosphorescence under activation by 365 nm UV light. Remarkably, the yellow afterglow remains visible to the naked eye under natural light conditions. Additionally, the transparency of this film allows the letters behind it to be visible under both visible and UV light conditions (Fig. 8(b)). Based on the above phenomenon, a mixture of molecule **C** (mass fraction of 6 %) and PVA was prepared to be used as a security ink. Then we wrote "DHU" on the filter paper. The letters depicted in Fig. 9 are invisible under natural light, but can be seen when exposed to the UV light. When the UV light is turned off, the letters exhibit a yellow phosphorescence. This obtained security ink holds promise for various applications, such as anti-counterfeiting or information encryption.

3 Conclusions

A series of phenanthroline-based D-A molecules are developed by expanding the conjugated molecular structure and replacing their substituent group which is conducive to the formation of the charge transport state. Benefiting from the heteroatom N of phenanthroline, these D-A molecules hold tremendous potential to generate the triplet exciton. Moreover, these heteroatoms

can establish hydrogen bonds with the polymer matrix, creating a rigid environment for the guest molecules and thereby inhibiting their NR relaxation process. When these D-A molecules are doped with PVA, the resulting doped films can be activated by 420 nm visible light, further generating RTP. A-PVA contain guest molecules which are composed of 2-hydroxybenzene and phenanthroline. Upon 365 nm UV irradiation, A-PVA-1 shows green RTP emission, and its phosphorescence lifetime τ reaches 140.41 ms. Compared with A-PVA, B-PVA and C-PVA contain guest molecules with larger conjugated structures and stronger D-A characteristics, resulting in a red-shifted emission. Additionally, their phosphorescence lifetime improved dramatically, with a maximum lifetime τ of 703.25 ms. When the UV light is turned off, both B-PVA and C-PVA exhibit yellow-green afterglow due to their dual vibrational peaks (green and yellow phosphorescence). Meanwhile, these films also can be activated by visible light. But their afterglow shows more yellowish under visible light activation because it is difficult to effectively activate the green phosphorescence with low-energy light. What is more, these films can be used for information encryption. In conclusion, we have successfully developed three flexible organic RTP materials with visible light-activated properties, and demonstrated their potential applications in information encryption and three-dimentional flexible light-emitting materials.

References

[1] TAN J, LI Q J, MENG S, et al. Time-dependent phosphorescence colors from carbon dots for advanced dynamic information encryption [J]. *Advanced Materials*, 2021, 33(16): e2006781.

[2] CHEN X Q, DAI W B, WU X H, et al. Fluorene-based host-guest phosphorescence materials for information encryption [J]. *Chemical Engineering Journal*, 2021, 426: 131607.

[3] WANG Y S, GAO H Q, YANG J, et al. High performance of simple organic phosphorescence host-guest materials and their application in time-resolved bioimaging [J]. *Advanced Materials*, 2021, 33(18): e2007811.

[4] XIAO F M, GAO H Q, LEI Y X, et al. Guest-host doped strategy for constructing ultralong-lifetime near-infrared organic phosphorescence materials for bioimaging [J]. *Nature Communications*, 2022, 13: 186.

[5] ZHOU T, WANG N, LI C H, et al. Sulfide sensor based on room-temperature phosphorescence of PbO/SiO_2 nanocomposite [J]. *Analytical Chemistry*, 2010, 82(5): 1705-1711.

[6] CAI S Z, SHI H F, TIAN D, et al. Enhancing ultralong organic phosphorescence by effective π-type halogen bonding [J]. *Advanced Functional Materials*, 2018, 28(9): 1705045.

[7] TIAN S, MA H L, WANG X, et al. Utilizing d-pπ bonds for ultralong organic phosphorescence [J]. *Angewandte Chemie International Edition*, 2019, 58(20): 6645-6649.

[8] GU L, SHI H F, BIAN L F, et al. Colour-tunable ultra-long organic phosphorescence of a single-component molecular crystal [J]. *Nature Photonics*, 2019, 13: 406-411.

[9] CHENG Z C, SHI H F, MA H L, et al. Ultralong phosphorescence from organic ionic crystals under ambient conditions [J]. *Angewandte Chemie International Edition*, 2018, 57(3): 678-682.

[10] GAN N, WANG X, MA H L, et al. Manipulating the stacking of triplet chromophores in the crystal form for ultralong organic phosphorescence [J]. *Angewandte Chemie International Edition*, 2019, 58(40): 14140-14145.

[11] HUANG Z Z, HE Z Y, DING B B, et al. Photoprogrammable circularly polarized phosphorescence switching of chiral helical polyacetylene thin films [J]. *Nature Communications*, 2022, 13: 7841.

[12] CAI S Z, MA H L, SHI H F, et al. Enabling long-lived organic room temperature phosphorescence in polymers by subunit interlocking[J]. *Nature Communications*, 2019, 10: 4247.

[13] YAN X, PENG H, XIANG Y, et al. Recent advances on host-guest material systems toward organic room temperature phosphorescence [J]. *Small*, 2022, 18(1): e2104073.

[14] ALAM P, LEUNG N L C, LIU J K, et al. Two are better than one: a design principle for ultralong-persistent luminescence of pure organics [J]. *Advanced Materials*, 2020, 32(22): e2001026.

[15] ZHANG Z Y, CHEN Y, LIU Y. Efficient room-temperature phosphorescence of a solid-state supramolecule enhanced by cucurbit[6]uril [J]. *Angewandte Chemie International Edition*, 2019, 58(18): 6028-6032.

[16] SUN S Y, WANG J, MA L W, et al. A universal strategy for organic fluid phosphorescence materials [J]. *Angewandte Chemie International Edition*, 2021, 60(34): 18557-18560.

[17] XIAO L, WU Y S, YU Z Y, et al. Room-temperature phosphorescence in pure organic materials: halogen bonding switching effects[J]. *Chemistry*, 2018, 24(8): 1801-1805.

[18] KWON M S, LEE D, SEO S, et al. Tailoring intermolecular interactions for efficient room-temperature phosphorescence from purely organic

materials in amorphous polymer matrices [J]. *Angewandte Chemie International Edition*, 2014, 53(42): 11177-11181.
[19] GAO Y F, ZHANG H L, SHUANG S M, et al. Visible-light-excited ultralong-lifetime room temperature phosphorescence based on nitrogen-doped carbon dots for double anticounterfeiting [J]. *Advanced Optical Materials*, 2020, 8(7): 1901557.
[20] LIU J W, MA Z M, LI Z W, et al. Crystal-state quad-mode triplet emissions of D-A-a'-D type phosphors with AIEE and visible-light-excited persistent phosphorescence [J]. *Dyes and Pigments*, 2021, 188: 109178.
[21] CAI S Z, SHI H F, LI J W, et al. Visible-light-excited ultralong organic phosphorescence by manipulating intermolecular interactions [J]. *Advanced Materials*, 2017, 29(35): 1701244.
[22] WU H W, CHI W J, CHEN Z, et al. Achieving amorphous ultralong room temperature phosphorescence by coassembling planar small organic molecules with polyvinyl alcohol [J]. *Advanced Functional Materials*, 2019, 29(10): 1807243.

由菲咯啉基分子与聚乙烯醇共组装的可见光活化磷光系统

张太广*，刘栋良，吴宏伟
东华大学 化学与化工学院，上海 201620

摘　要：开发可见光活化的纯有机室温磷光（room-temperature phosphorescence，RTP）材料已引起广泛关注。通过将基于菲咯啉的供体-受体（donor-acceptor，D-A）荧光粉掺入刚性聚合物基质聚乙烯醇（polyvinyl alcohol，PVA）中，开发了一种可见光激活的 RTP 设计策略。富含杂原子 N 的菲咯啉可促进三重态激子的产生，并与 PVA 形成丰富的氢键，抑制非辐射弛豫，从而引发磷光。在 420 nm 可见光照射下，通过调节分子共轭结构和 D-A 相互作用，掺杂荧光粉的 PVA 薄膜的磷光颜色可从绿色变为黄色。基于上述磷光特性，该薄膜可用于信息加密。该研究为在信息加密、传感器等领域制备具有良好应用前景的可见光活化磷光材料提供了一种简单可行的方法。

关键词：磷光；菲咯啉；可见光；聚合物体系